nature astronomy

LETTERS

https://doi.org/10.1038/s41550-018-0541-x

Astronomical detection of radioactive molecule ^{26}AlF in the remnant of an ancient explosion

Tomasz Kamiński[1]*, Romuald Tylenda[2], Karl M. Menten[3], Amanda Karakas[4], Jan Martin Winters[5], Alexander A. Breier[6], Ka Tat Wong[5], Thomas F. Giesen[6] and Nimesh A. Patel[1]

Decades ago, γ-ray observatories identified diffuse Galactic emission at 1.809 MeV[1–3] originating from β^+ decays of an isotope of aluminium, ^{26}Al, that has a mean lifetime of 1.04 million years[4]. Objects responsible for the production of this radioactive isotope have never been directly identified owing to insufficient angular resolutions and sensitivities of the γ-ray observatories. Here, we report observations of millimetre-wave rotational lines of the isotopologue of aluminium monofluoride that contains the radioactive isotope (^{26}AlF). The emission is observed towards CK Vul, which is thought to be a remnant of a stellar merger[5–7]. Our constraints on the production of ^{26}Al, combined with the estimates on the merger rate, make it unlikely that objects similar to CK Vul are major producers of Galactic ^{26}Al. However, the observation may be a stepping stone for unambiguous identification of other Galactic sources of ^{26}Al. Moreover, a high content of ^{26}Al in the remnant indicates that, before the merger, the CK Vul system contained at least one solar-mass star that evolved to the red giant branch.

Historic records[8,9] show that CK Vul or Nova 1670 underwent an unusual outburst in 1670–1672. It was similar to outbursts of objects known as red novae, which erupt in a stellar merger before cooling off to low temperatures[10,11]. In this cool phase, they produce large amounts of molecular gas and dust. CK Vul was recently discovered to be associated with a significant amount of dust and molecular gas as well[12]. What distinguishes CK Vul, even among red novae, is a high abundance of isotopes that are rare in matter of normal cosmic composition[5,12]. In particular, our observation of ^{26}AlF in four rotational transitions (Fig. 1 and Methods) is a firm detection of a radioactive molecule in CK Vul. This discovery follows numerous unsuccessful attempts to detect ^{26}AlF in astronomical objects[13–15]. The unstable nucleus of ^{26}Al is virtually absent in solar-composition objects and has a modest abundance of 10^{-5} with respect to ^{27}Al in the Galactic interstellar medium, whereas in CK Vul it is only ~7 times less abundant than the stable isotope ^{27}Al (Methods).

The molecular remnant of CK Vul was discovered at millimetre wavelengths in rotational emission lines from a large variety of molecules[5,12]. Imaging has shown that the CO emission region has an extent of ~13″, a morphology of bipolar lobes and a torus-like feature, which all are located at a centre of a much larger (71″) bipolar optical nebula of recombining plasma[5,16]. The main AlF emission is observed in a small region of a full-width-at-half-maximum size of $1.80\,(\pm0.05)\times0.84\,(\pm0.06)$ arcsec, with the major axis at a position angle of 60° (±1°) and centred close to the radio-continuum source of CK Vul[16]. At a distance of 0.7 kpc[17], the maximum extent corresponds to an e-folding radius of 430 AU. The AlF emission appears as a pair of two axisymmetric and collimated streams emanating from the centre of the remnant and heading towards the north-eastern and south-western walls of lobes seen in CO and continuum dust emission (Fig. 2). Additionally, our most sensitive observations trace weak ^{27}AlF emission, at a level of 3% of the peak, within the lobes out to a radius of 5.5 arcsec. The emission lines have an intrinsic full width of ~140 km s^{-1}, which is smaller than that of most other species observed in this source[12]. The north-eastern part of the AlF region contributes most to the redshifted emission, and the opposite side dominates the blueshifted emission, consistent with the overall kinematics of the molecular remnant.

Among all the molecular species that have been mapped thus far in CK Vul (examples of which are shown in Supplementary Fig. 1; also see Supplementary Table 2), the AlF emission has a unique distribution. That we observe the radioactive molecule of ^{26}AlF only in a small region of the remnant is probably a chemical effect related to the formation and destruction of AlF. Observations of the AlF molecule in circumstellar media are rare but suggest that AlF forms close to stellar photospheres (that is, at relatively high densities)[18,19]. Shocks and dust sputtering were also considered as a source of AlF[20]. None of the scenarios can be excluded for CK Vul. The synthesis of AlF is probably limited by the elemental abundance of fluorine, not aluminium[18]. The remnant can therefore contain other atomic and molecular forms of aluminium—some possibly depleted into dust. Thus, our AlF observations constrain only a lower limit on the content of ^{26,27}Al in CK Vul. A search of other probable molecular carriers of aluminium (for example, AlCl, AlO, AlOH and AlCN) has been performed[12], but none has been detected, suggesting a small reservoir of aluminium-bearing molecules other than AlF. In contrast, a contribution from atomic aluminium to the recombining nebula may be significant. There are currently no observations that could be used to verify whether atomic aluminium is present. Based on the excitation analysis presented in the Methods, we derive a total mass of the observed ^{26}Al of $(3.4\pm1.8)\times10^{24}$ g, which is equivalent to about a quarter of the mass of Pluto.

The ^{26}Al isotope is produced in the Mg–Al cycle in hydrogen burning via the ^{25}Mg(p, γ)^{26}Al reaction, which requires temperatures above 30×10^6 K[21]. It is thought to be efficiently produced in a variety of stars, including: classical novae with O–Mg–Ne white dwarfs; Wolf–Rayet stars; core-collapse supernovae; and asymptotic giant branch (AGB) stars that experienced hot bottom burning[3,22]. The progenitor of CK Vul was neither of these objects[5,17,23]. However,

[1]Harvard-Smithsonian Center for Astrophysics, Cambridge, MA, USA. [2]Department for Astrophysics, Nicolaus Copernicus Astronomical Center, Toruń, Poland. [3]Max-Planck-Institut für Radioastronomie, Bonn, Germany. [4]Monash Centre for Astrophysics, School of Physics and Astronomy, Monash University, Clayton, Victoria, Australia. [5]IRAM, Domaine Universitaire de Grenoble, Grenoble, France. [6]Laborastrophysik, Institut für Physik, Universität Kassel, Kassel, Germany. *e-mail: tkaminsk@cfa.harvard.edu

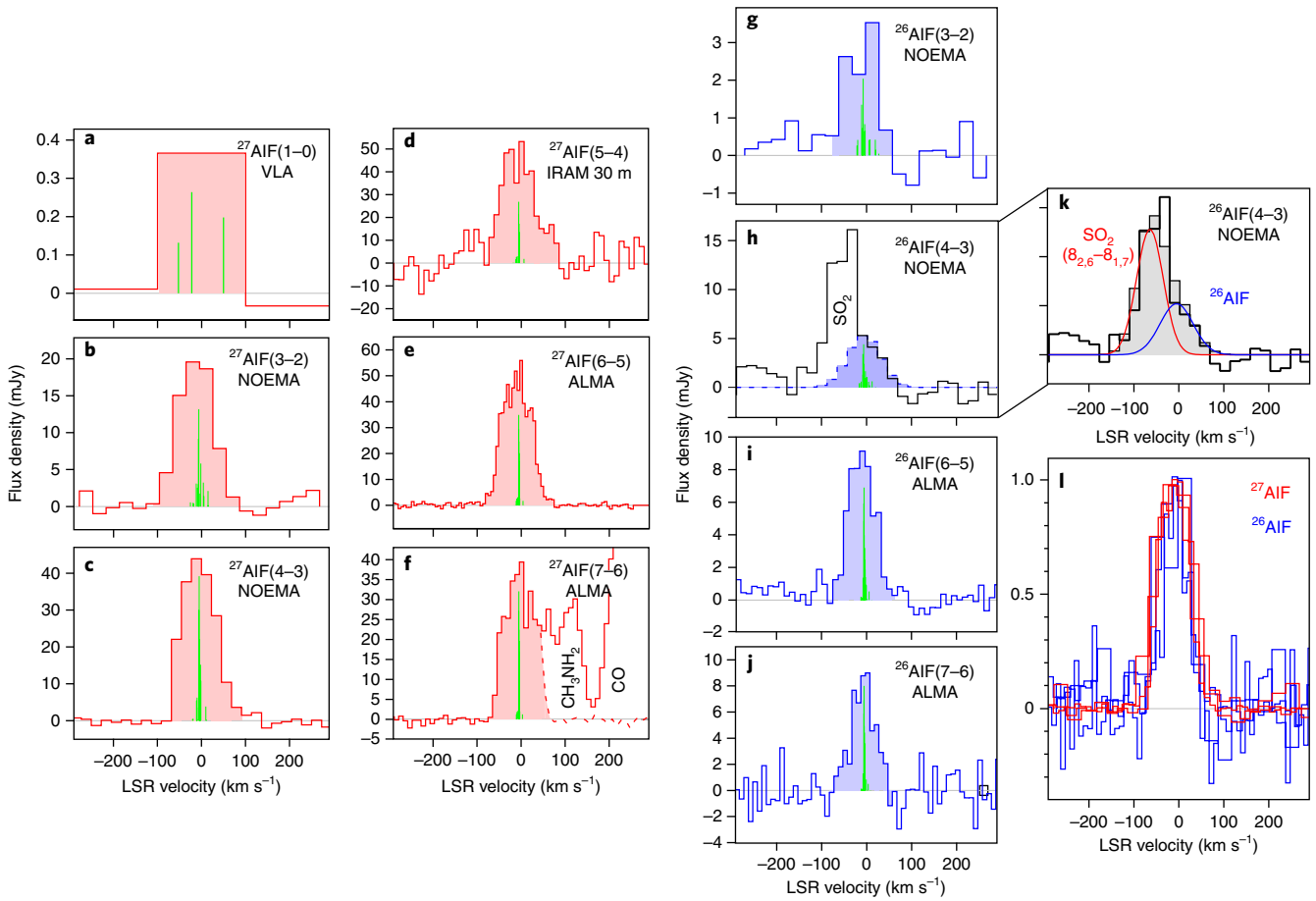

Fig. 1 | Spectra of rotational lines of AlF in CK Vul. Spectra are displayed in the local standard of rest (LSR) frame. **a**–**j**, Green vertical lines illustrate the hyperfine structure of the transitions (in arbitrary intensity units). Areas shaded in red and blue show the ^{27}AlF (**a**–**f**) and ^{26}AlF emissions (**g**–**j**), respectively, and represent the main emission region of AlF. Some spectra were smoothed in resolution, most heavily for ^{27}AlF $J=1$–0, which was observed with the Karl G. Jansky Very Large Array (VLA). The transition and telescope used to collect the data are indicated in each panel. For lines observed with a single-dish telescope and with an interferometer, only the interferometric spectrum is shown. In **f**, the ^{27}AlF 7–6 transition is contaminated by emission of methylamine, and a mirrored profile is shown with a dashed line to illustrate the contribution of ^{27}AlF. **k**, The feature shown with a black empty histogram was decomposed into two Gaussians corresponding to SO_2 (red) and ^{26}AlF (blue). The shaded grey histogram shows the best-fitting combined profile. **l**, Normalized profiles of unblended lines observed with interferometers are overlaid to illustrate their close alignment. Red lines correspond to transitions of ^{27}AlF, while blue lines are for ^{26}AlF.

more ordinary low-mass stars can produce ^{26}Al as well. The ^{26}Al synthesis takes place on the red giant branch (RGB) when hydrogen is burnt in a shell surrounding a helium core. Our model simulations (see ref. [24] and Methods) show that the most favourable conditions for producing ^{26}Al occur when a star develops a condensed degenerate core; that is, for initial stellar masses 0.8–2.5$M_\odot$. The ^{26}Al isotope is then deposited in a narrow outermost layer of the helium core (Fig. 3). In a single RGB star, envelope convection never reaches the helium core; therefore, there is no way to dredge ^{26}Al up to the stellar surface (and disperse it into the circumstellar and interstellar media). However, if the star is in a binary system and collides with a companion, matter from the interiors of both stars can be mixed and ejected into the circumstellar medium. In particular, if the companion has a condensed core, the ^{26}Al-rich outer layers of the helium core of the RGB primary can be disrupted and exposed, to eventually form a remnant such as that of CK Vul. Only a small portion of the available ^{26}Al would have to be dispersed to explain the observed mass of ^{26}Al and the aluminium isotopic ratio measured in CK Vul. Our calculations show that stars of 0.8–2.5$M_\odot$ store a few times 10^{27} g of ^{26}Al in the outermost layers of the helium core (that is, a factor of 1,000 more than that found in CK Vul). Given this result and other observational constrains, a merger of two low-mass stars with at least one being on the RGB is the most likely scenario to explain CK Vul. Population-synthesis studies indeed indicate that low-mass binaries evolving off the main sequence to the RGB (and with orbital periods of 1−30 d) have a high chance of merging[25,26].

The ^{26}Al decays are followed by emission of energetic positrons, which may be an important local ionization source in CK Vul. Following Glassgold[27], our results suggest a ^{26}Al-induced ionization rate of 2.0×10^{-16} s^{-1} per hydrogen nucleus for CK Vul. This is a lower limit considering that the derived ^{26}Al mass is a lower limit and we adopted the solar elemental abundance for an object where aluminium is probably enhanced[12]. The derived rate is the same as the typical ionization rate by cosmic rays in the Galactic Disk[28]. The regions of strong emission in the two ions (N_2H^+ and HCO^+) that were observed in CK Vul simultaneously with AlF are more extended than that of ^{26}AlF (Supplementary Fig. 1), suggesting that additional ionization mechanisms are active in the remnant. It is possible that atomic forms of the radioactive nuclide of aluminium extend and ionize the remnant beyond the region traced in ^{26}AlF emission, or that other radioactive species are present in the remnant.

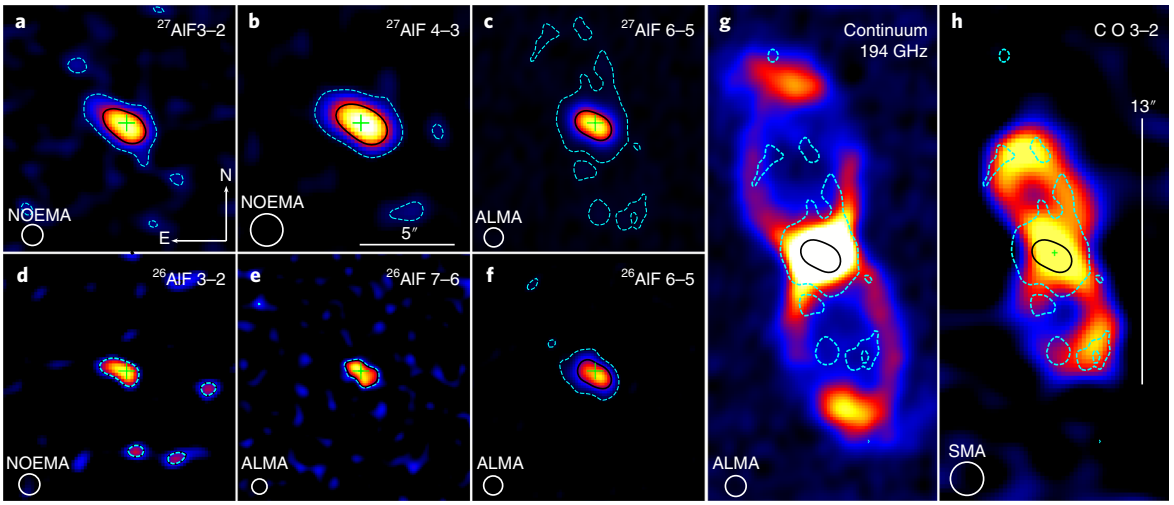

Fig. 2 | Maps of molecular emission of ^{26}AlF and ^{27}AlF. a–f, Images and contours of emission in different transitions of ^{27}AlF (**a**–**c**) and ^{26}AlF (**d**–**f**), as indicated by the labels in the top-right corners. The black contour is drawn at half the peak flux and the dashed cyan contour represents emission at the 3σ level. The contours overlap in **d** and **e**. **g**,**h**, Comparison of the AlF 6–5 contours (from **c**) with the map of continuum emission (**g**) and that of CO 3–2 (**h**). All the colour images show flux at different linear scales. Crosses indicate the position of the radio source.

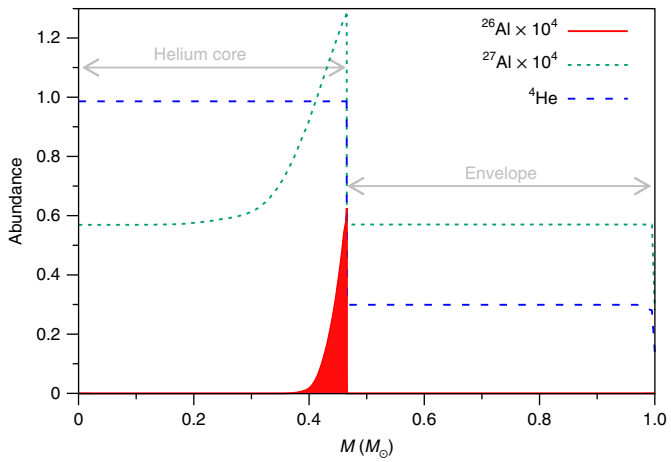

Fig. 3 | Mass-abundance profiles of He, ^{26}Al and ^{27}Al in a model of a 1$M_\odot$ star at the tip of the RGB. The abundance of helium (blue line) defines the extent of the helium core and the hydrogen envelope, which are labelled. The abundances of ^{26}Al (red shaded area) and ^{27}Al (green dashed line) were scaled by a factor of 10^4.

From the intensity of the 1.8 MeV line, it was estimated that all Galactic sources produce 1–3$M_\odot$ of ^{26}Al every 1 Myr[1,2,29]. With our estimates of the ^{26}Al mass in CK Vul, one would need ~1,100 mergers like CK Vul going off every year to explain the entire Galactic content of ^{26}Al. This figure is unrealistic as current rates of red novae suggest one to two such energetic transients per decade[26], and the rates are probably even lower for eruptions more characteristic of CK Vul[7]. In contrast, if the mass of ^{26}Al in CK Vul is underestimated by a factor of 1,100—for example, by not accounting for ^{26}Al present in the atomic phase, other molecules and solids—objects like CK Vul may be important contributors to the Galactic production of this radioactive nuclide. More observations and realistic models of the ionization and chemical structure of the remnant are necessary to investigate this issue further.

The 1.8 MeV emission arising from ^{26}Al decays is hardly absorbed by interstellar or circumstellar matter[27] and easily escapes from the compact ^{26}AlF region, even though it is heavily obscured by dust and gas (Fig. 2). Using our ^{26}AlF observational constraints as a lower limit on the ^{26}Al content in CK Vul, we calculate that the ^{26}Al decay line has a flux of $\gtrsim 1.6\times10^{-10}$ cm^{-2} s^{-1}, which is much below the sensitivity limit of the contemporary Spectrometer on INTEGRAL (SPI; ~10^{-5} cm^{-2} s^{-1} in a 10^6 s integration)[30]. At such low estimated flux, it will be challenging to detect the 1.8 MeV line from CK Vul, and probably from any other single stellar source, even with future more sensitive γ-ray instruments. However, the case of CK Vul illustrates that millimetre-wave spectroscopy performed by the Atacama Large Millimeter/submillimeter Array (ALMA) and Northern Extended Millimeter Array (NOEMA) can now be used to study Galactic sources of radioactive nuclides, provided they produce molecules. Modern interferometer arrays can not only detect but also spatially identify discrete objects that are actively enhancing the Galaxy in ^{26}Al. Because observations of molecules yield relatively easily the isotopologue (and thus isotopic) ratios, which are not available through γ-ray observations, millimetre-wave spectroscopy also has the potential to better identify the nucleosynthesis processes that lead to the Galactic ^{26}Al production.

Methods

Spectroscopic data for AlF isotopologues. The identification and analysis of the pure rotational emission of ^{26}AlF and ^{27}AlF was based on spectroscopic data prepared in this study. For ^{27}AlF, we used mass-scaled Dunham parameters and hyperfine constants derived from laboratory measurements[31]. Accurate line positions of ^{26}AlF were calculated through the mass-scaled Dunham parameters of ^{27}AlF. We used fourth-order correction terms to derive positions of hyperfine components with an accuracy better than 1 MHz. The hyperfine splitting of ^{26}AlF is more complex than that of ^{27}AlF owing to a twice larger nuclear spin (I=5). To derive the hyperfine structure for ^{26}AlF, we used higher-order Dunham corrections and scaled accordingly the ^{26}Al electric quadrupole moment Q[31] and the magnetic coupling parameter c_I with the nuclear g_N factor. A permanent dipole moment of μ=1.53 D[32] was adopted for both isotopologues. The spectroscopic constants we used to generate the line lists are given in Supplementary Table 1. Line frequencies, energies of the rotational levels above the ground (E_u), line strengths ($S_u l\mu^2$) and partition functions were derived using pgopher[32]. The method of our calculations is similar to that used in earlier studies of rotational spectra of ^{26}AlF[14].

Spectroscopic laboratory studies of rare radioactive materials such as ^{26}AlF would be very challenging. Although laboratory measurements are usually needed to unambiguously identify complex molecules, it is not necessary for simple diatomic species, especially for most astronomical applications. For diatomic molecules and within the Born–Oppenheimer approximation, the mass dependence of spectra can be separated from that of the bond length. The underlying theory was developed by Dunham in 1932[33] and has been successfully applied to many molecules. The spectra of diatomic molecules of identical

bond length differ only in the mass scaling factors, which are known to a high accuracy. Measurements for one isotopic species (for example, $^{27}Al^{19}F$) are thus sufficient to determine spectra of other isotopologues (for example, $^{26}Al^{19}F$). High-precision measurements of different isotopologues can show how accurate this approximation is, and higher-order corrections, if necessary, can be added. The corrections are often insignificant; in particular, they are typically much smaller than the accuracy of astronomical observations[34]. Our calculations included these corrections but they turned out to be negligible in the case of the studied source, whose line widths are of ~140 km s^{-1}.

Because the AlF lines are so intrinsically broad in CK Vul, their hyperfine structure is unresolved in most of our observations. As shown in Fig. 1, the hyperfine splitting is highest in the $J=1$–0 transition; however, this was observed at insufficient sensitivity to reveal the hyperfine structure (and is degraded in resolution in the figure). For both isotopologues, the hyperfine splitting caused by the ^{19}F nucleus is negligible. The full spectroscopic data, which include the hyperfine splitting of $^{26}Al^{19}F$ and uncertainties in line positions, are available in electronic form in CDS at http://cdsarc.u-strasbg.fr/viz-bin/qcat?J/other/NatAs/. In our analysis, we often used the intensity-weighted mean frequency and the sum of line strengths $S_u\mu^2$ to represent the position and strength of a given transition, respectively. The centroid line frequencies and line strengths used in the analysis are given in Supplementary Table 2.

Single-dish observations. The presence of ^{27}AlF in CK Vul was revealed in the line survey obtained with the Institut de Radioastronomie Millimétrique (IRAM) 30 m and Atacama Pathfinder Experiment 12 m (APEX) telescopes in 2014–2017[12]. The survey provided measurements of ^{27}AlF emission in the following transitions: $J=3$–2, 4–3, 5–4 and 6–5. Additionally, the 7–6 transition was covered by IRAM 30 m spectra, but it overlaps with a much stronger line of CO $J=2$–1 and its flux could not be reliably measured. Two other lines of ^{27}AlF (that is, $J=8$–7 and 9–8) were covered but not detected. Their upper 5σ limits and the fluxes of the other detected lines are given in Supplementary Table 2.

Most of the corresponding transitions of ^{26}AlF were also covered in the survey. We find a weak spectral feature at the expected location of ^{26}AlF 3–2, but the emission line partially overlaps with a broader instrumental feature[12]. The 4–3 line is also visible and it partially overlaps with the $J_{K_a,K_c}=8_{2,6}$–$8_{1,7}$ line of SO_2 (see below). Only rough flux constraints on the ^{26}AlF 4–3 emission could be obtained from this blending feature. The $J=5$–4 transition of ^{26}AlF overlaps with a much stronger line of $H^{13}C^{15}N$ 2–1 and the flux contribution of ^{26}AlF could not be assessed. Another covered line, $J=7$–6, appears to be clear of any contamination but is seen at a modest ~3σ level. All other lines are below our sensitivity limits. The three ^{26}AlF features (that is, $J=3$–2, 4–3 and 7–6) are observed at a modest signal-to-noise ratio (S/N) and their observations alone constitute only a tentative indication of the presence of ^{26}AlF in CK Vul. The three features, however, provided a strong incentive to repeat the observations with more sensitive interferometers.

Interferometric observations. The sensitive observations of both AlF isotopologues were obtained with the Karl G. Jansky Very Large Array (VLA), NOEMA and ALMA. The interferometric observations are summarized in Supplementary Table 3. The line fluxes are given in Supplementary Table 2. The following transitions were observed:

- The $J=1$–0 transitions of ^{26}AlF and ^{27}AlF were covered by a K_a band spectrum obtained with the JVLA in the DnC configuration. The lowest transition of AlF has a significant hyperfine splitting that is comparable to the intrinsic line width of AlF emission (Fig. 1a). This extra broadening makes the line peak intensity lower and harder to detect than for lines at higher frequencies. Only after smoothing the spectrum to a resolution comparable to the hyperfine splitting is the emission of ^{27}AlF 1–0 apparent (Fig. 1a). This transition should be considered as only tentatively detected. The flux of the line is at a 2–5σ level, which is insufficient to provide a good-quality map of the ^{27}AlF 1–0 emission. To extract the spectrum, we used an aperture defined in maps of ^{27}AlF 3–2 from NOEMA. The ^{26}AlF 1–0 emission is not detected in the JVLA data, consistent with the isotopologue ratio derived in this study.
- The $J=3$–2 transition of both AlF isotopologues was observed with the emerging NOEMA interferometer. Observations were obtained in 2016 and 2017 with seven and eight antennas, respectively. The WideX correlator was used. Both transitions are detected and their emission regions resolved with a beam of ~0.78 arcsec. At this angular resolution, the peak signal-to-noise values of the two emission regions are 24 and 5 (and higher for source-averaged fluxes).
- The $J=4$–3 transitions were observed with six antennas of NOEMA and with WideX. The ^{27}AlF emission region is marginally resolved by the beam of ~1.64 arcsec. The ^{27}AlF emission may be contaminated by the HNCO $6_{0,6}$–$5_{0,5}$ line whose rest frequency is 29.7 km s^{-1} away from that of ^{27}AlF 4–3. The separation is smaller than the full width at half maximum of the observed feature of 40.8 km s^{-1}. An excitation model of HNCO based on the single-dish survey[12] implies that less than 6% of the total flux of the observed feature may come from HNCO. However, the accuracy of this model is modest and the model does not take into account the potential difference in spatial distributions of HNCO and AlF emission. The characteristics of the emission region ascribed here to ^{27}AlF 4–3 are the same as those of other AlF transitions and do not indicate any sign of contamination. We therefore neglect the potential contribution from HNCO and interpret the total flux of the emission feature as that of ^{27}AlF 4–3. The corresponding ^{26}AlF 4–3 transition is detected by NOEMA but blends partially with the SO_2 $8_{2,6}$–$8_{1,7}$ line whose rest frequency is blueshifted by 55.9 km s^{-1} with respect to the ^{26}AlF line. Interferometric ALMA imaging of another line of SO_2, $4_{2,2}$–$3_{1,3}$, shows that the extent of the emission region of SO_2 is similar to that of AlF (Supplementary Fig. 1); therefore, the relative contribution of the two species to the blend cannot be disentangled based on spatial information alone. However, the kinematic separation of the SO_2 and ^{26}AlF lines is wide enough to perform a de-blending procedure in which the best-fitting combination of two Gaussian components gives the line characteristics. The line centres were fixed while the amplitudes and widths were free parameters in this χ^2 minimization procedure. The results are shown in Fig. 1h–j, and the flux of ^{26}AlF 4–3 is given in Supplementary Table 2. The flux of the SO_2 line is 2.34 times higher than that of ^{26}AlF.
- Both isotopologues were observed with ALMA in the $J=6$–5 lines located in ALMA Band 5. These are the most recent observations (April 2018) and provided us with spectra and maps of the best sensitivity. At a beam size of 1.4 × 1.1 arcsec (at natural weighting), both emission regions are resolved and their peaks are observed at S/N values of 170 and 33 (the source-averaged fluxes give even higher S/Ns).
- The $J=7$–6 transition of both isotopic species was observed with ALMA in Band 6. Both lines are observed at a high S/N and are well resolved with a 0.8 arcsec beam. The ^{27}AlF line overlaps with a broad wing of an intense line of CO 2–1. The location of the ^{27}AlF 7–6 line corresponds to a velocity of 333 km s^{-1} with respect to the centre of the CO 2–1 emission. At this velocity, the CO emission is relatively faint and extended (that is, most of the CO emission is spread over a region of a radius of ~6 arcsec from the centre of the molecular remnant). Our maps of AlF transitions, including the map of ^{26}AlF 7–6 from the same ALMA dataset, show that the AlF emission is enclosed within a radius of 1.05 arcsec. Hence, by extracting the signal within the AlF emission region defined in other observations, we minimized the contamination from the CO emission. Furthermore, the spectrum extracted within the AlF emission region reveals that the ^{27}AlF 7–6 transition partially overlaps with an emission feature that we tentatively identify as a transition of methylamine, CH_3NH_2 $3_{2,4}$–$3_{1,5}$, whose rest frequency is 140 km s^{-1} away from that of ^{27}AlF 7–6. To measure the pure flux of ^{27}AlF 7–6, we replaced the small contaminated part of its original profile with the mirrored unaffected wing, as shown in Fig. 1f. A flux measured in such a modified profile is given in Supplementary Table 2.

The line positions, line widths, sizes and shapes of the emission regions are consistent between the different transitions, leaving no doubt about their identification as ^{27}AlF and ^{26}AlF. In particular, the consistency in the spatial distribution of the emission assigned to ^{26}AlF with that of ^{27}AlF indicates that it must be an isotopologue of AlF—no other species observed in CK Vul has a spatial distribution identical to that of AlF, which is illustrated in Supplementary Fig. 1. The uncertainty in the calculated positions of the ^{26}AlF lines of ~1 MHz is insignificant compared with the observed linewidths of approximately 50–120 MHz, and the predicted line positions are in excellent agreement with the centres of the emission lines assigned to ^{26}AlF (in the rest frame of the object). The match between the calculated and observed line positions of ^{26}AlF is as good as for ^{27}AlF (Fig. 1), whose rotational spectra were measured in a laboratory. Also, within the observation errors, the line intensities of ^{26}AlF are consistent with excitation under thermal equilibrium conditions, and the excitation temperature of ^{26}AlF is consistent with that of ^{27}AlF (see below). In the 7.75 GHz wide spectrum acquired with ALMA in Band 6, we observe only four features of similar intensity and width as those of ^{26}AlF 7–6. Within the accuracy to which we can determine the observed line positions in CK Vul, the ALMA Band 6 spectrum indicates a probability of a chance coincidence of 1:840. A probability that all 4 lines match the calculated frequencies is smaller than 10^{-11}. Therefore, a false identification is highly unlikely.

The spectra acquired to secure the AlF observations serendipitously covered transitions of other species. Additionally, we observed CK Vul with NOEMA in two frequency setups centred at about 89.3 and 146.0 GHz to map emission of species other than AlF. Interferometric imaging of molecular emission was also obtained with the Submillimeter Array (SMA) and reported earlier[5]. Supplementary Table 3 contains details of these complementary observations and provides a list of the main lines that were observed. All the interferometric observations allowed us to measure continuum emission. All these extra materials allowed us to trace the complex kinematical, chemical and excitation structure of the molecular remnant and thus provided an important context for the interpretation of the AlF emission.

All the interferometric data were calibrated using standard procedures. ALMA and NOEMA data were additionally self-calibrated on the strong continuum source. Continuum emission was subtracted from the visibilities as a zeroth- or first-order polynomial fitted to the full band and avoiding strong lines. Interferometric maps presented here were obtained in CASA[35] and using CLEAN. The weighting of visibilities—natural or robust—was adjusted to the aims of the analysis. We often used images with a restoring beam of a circular shape and of a diameter equal to the geometric mean of the 'dirty' beam size.

Excitation analysis and determination of the isotopic ratio. The excitation temperature and column densities of the AlF isotopologues were derived in a population-diagram analysis[36]. The population diagram is shown in Supplementary Fig. 2. We used a Python's *emcee* implementation[37] of the Markov chain Monte Carlo method[38] to obtain linear fits to the data. In the associated error analysis, we considered statistical uncertainties from the thermal noise in the flux measurements and 20% systematic errors in the flux calibrations. We assumed that both isotopologues are located in the same volume and have the same single excitation temperature. That the temperatures are, within uncertainties, equal for both species is evident from the same slopes of lines that can be fitted to both sets of points independently. The source size of 1.80×0.84 arcsec was used to calculate the beam filling factors. This size is a weighted mean of all beam-deconvolved sizes measured in our ^{26}AlF and ^{27}AlF maps. Free parameters of the population-diagram fit were the excitation temperature (T_{ex}), column density of ^{27}AlF (N_{27}) and ratio of the column density of ^{27}AlF to that of ^{26}AlF (N_{27}/N_{26}). We used uniform ('uninformative') priors for the three parameters, allowing their values to be in arbitrary but reasonably broad ranges. A few thousand 'walkers' were used in *emcee* to derive the posterior distributions. After the first determination of the column densities, we calculated the line opacities and corrected the measured fluxes for the corresponding saturation[38]. The calculation of the free parameters was then repeated. The maximum optical thickness in this second iteration was $\tau_{max}=0.3$. The saturation correction is only 1.4% higher than in the previous iteration and no further corrections were applied. The procedure yielded $T_{ex}=12.9^{+2.4}_{-1.8}$ K, $N_{27}=3.0^{+0.6}_{-0.5}\times10^{15}$ cm^{-2} and $N_{27}/N_{26}=7.1^{+3.2}_{-2.2}$, where the median values are associated with uncertainties corresponding to 97.3% confidence levels. These uncertainties are underestimated and do not take into account, for instance, errors in the source size.

The population-diagram analysis relies on the assumption of thermodynamic equilibrium in the gas. The assumption is not granted in CK Vul considering that some species appear to be subthermally excited[12]. However, the AlF population diagram itself does not indicate any strong deviations from what is expected in thermodynamic equilibrium. Also, the excitation temperature of AlF derived here is consistent with the kinetic temperature constrained from the single-dish survey[12]. Using collision rates of AlF with *para*-H_2 and with helium at 10 K[39,40], we calculated critical densities for all observed transitions. They range from 10^4 cm^{-3} for $J=1$–0 to 10^7 cm^{-3} for $J=7$–6 and are therefore comparable to critical densities of analogous transitions of low-density molecular tracers such as CO. The AlF gas is probably thermalized and the level populations are probably close to thermodynamic equilibrium.

Nucleosynthesis of ^{26}Al. To investigate the synthesis of ^{26}Al in low-mass stars evolving off the main sequence to RGB, we analysed state-of-the-art solar-metallicity evolutionary sequences calculated with the Monash stellar-evolution code[41]. The surface abundances on the AGB were investigated with the code described in ref. [43]. The models are evolved from the zero-age main sequence to near the end of the thermally pulsing AGB phase. For the purposes of this study, we sampled the interior composition of the star at the tip of the RGB before core helium burning is ignited. The grid includes models between 1 and 8$M_\odot$ and we considered models for 1–3$M_\odot$ for this study. The nuclear network and initial abundances used for the nucleosynthesis calculations are described in ref. [44] and the input physics used in the stellar-evolutionary calculations are described in ref. [43]. Evolution of a grid of low-mass stars (0.9–3.0$M_\odot$) from the pre-main-sequence up to the helium flash (end of the red giant phase) was also performed using the TYCHO (version 6.0) stellar-evolution code developed by Arnett and collaborators[42].

We find that for all the considered models, the mass of ^{26}Al increases with the time spent on the RGB. The abundance profiles of the aluminium isotopes at the tip of the RGB (Fig. 3) indicate a high content of ^{26}Al only in the outermost parts of the well-developed helium core. There is not much difference between the amount of ^{26}Al synthesized in 1 and 2$M_\odot$ models, but the total ^{26}Al mass becomes smaller in models of stars of higher masses. For instance, the total mass of ^{26}Al in the 1$M_\odot$ model is 9×10^{27} g, and in the 3$M_\odot$ model it is only 4×10^{26} g. The lower production of ^{26}Al in the more massive stars is related to their relatively short time spent on the RGB. Also, stars with initial masses of $\geq2.5M_\odot$ burn hydrogen on the main sequence in a convective core, which eventually results in a lower temperature of hydrogen shell burning on the RGB, and consequently a lower production of ^{26}Al. We therefore consider 2.5$M_\odot$ as an upper limit on the mass of the CK Vul's progenitor. Stars with masses $\lesssim0.8M_\odot$ evolve longer than the age of the Universe and could not have produced sufficient ^{26}Al to explain our observations of CK Vul, setting an approximate lower mass limit on the progenitor.

Data availability. Raw and processed ALMA data that support the findings of this study are accessible in the ALMA archive (http://almascience.nrao.edu/aq/). These and other astronomical data are also available from the corresponding author upon reasonable request. The electronic table containing the calculated hyperfine structure of ^{26}AlF transitions is available at CDS: http://cdsarc.u-strasbg.fr/viz-bin/qcat?J/other/NatAS.

Received: 4 February 2018; Accepted: 2 July 2018;
Published online: 30 July 2018

References

1. Mahoney, W. A., Ling, J. C., Jacobson, A. S. & Lingenfelter, R. E. Diffuse galactic gamma-ray line emission from nucleosynthetic Fe-60, Al-26, and Na-22—preliminary limits from HEAO 3. *Astrophys. J.* **262**, 742 (1982).
2. Mahoney, W. A., Ling, J. C., Wheaton, W. A. & Jacobson, A. S. HEAO 3 discovery of Al-26 in the interstellar medium. *Astrophys. J.* **286**, 578 (1984).
3. Diehl, R. et al. COMPTEL observations of Galactic ^{26}Al emission. *Astron. Astrophys.* **298**, 445 (1995).
4. Samworth, E. A., Warburton, E. K. & Engelbertink, G. A. P. Beta decay of the ^{26}Al ground state. *Phys. Rev. C* **5**, 138–142 (1972).
5. Kamiński, T. et al. Nuclear ashes and outflow in the eruptive star Nova Vul 1670. *Nature* **520**, 322–324 (2015).
6. Kato, T. CK Vul as a candidate eruptive stellar merging event. *Astron. Astrophys.* **399**, 695–697 (2003).
7. Tylenda, R. et al. OGLE-2002-BLG-360: from a gravitational microlensing candidate to an overlooked red transient. *Astron. Astrophys.* **555**, A16 (2013).
8. Hevelius, J. An extract of a letter, written to the publisher by the excellent Johannes Hevelius, concerning his further observations of the new star near the beak of the Swan. *Phil. Trans. R. Soc. Lond. I* **6**, 2197 (1671).
9. Shara, M. M., Moffat, A. F. J. & Webbink, R. F. Unraveling the oldest and faintest recovered nova—CK Vulpeculae (1670). *Astrophys. J.* **294**, 271–285 (1985).
10. Tylenda, R. & Soker, N. Eruptions of the V838 Mon type: stellar merger versus nuclear outburst models. *Astron. Astrophys.* **451**, 223–236 (2006).
11. Tylenda, R. et al. V1309 Scorpii: merger of a contact binary. *Astron. Astrophys.* **528**, AA114 (2011).
12. Kamiński, T. et al. Organic molecules, ions, and rare isotopologues in the remnant of the stellar-merger candidate, CK Vulpeculae (Nova 1670). *Astron. Astrophys.* **607**, A78 (2017).
13. Oberlack, U. et al. COMPTEL limits on ^{26}Al 1.809 MeV line emission from γ2 Velorum. *Astron. Astrophys.* **353**, 715–721 (2000).
14. Guelin, M. et al. Nucleosynthesis in AGB stars: observation of ^{25}Mg and ^{26}Mg in IRC+10216 and possible detection of ^{26}Al. *Astron. Astrophys.* **297**, 183–196 (1995).
15. Banerjee, D. P. K. et al. A search for radioactive ^{26}Al in the nova-like variable V4332 Sagittarii. *Astrophys. J.* **610**, L29–L32 (2004).
16. Hajduk, M. et al. The enigma of the oldest 'nova': the central star and nebula of CK Vul. *Mon. Not. R. Astron. Soc.* **378**, 1298–1308 (2007).
17. Hajduk, M., van Hoof, P. A. M. & Zijlstra, A. A. CK Vul: evolving nebula and three curious background stars. *Mon. Not. R. Astron. Soc.* **432**, 167–175 (2013).
18. Highberger, J. L., Savage, C., Bieging, J. H. & Ziurys, L. M. Heavy-metal chemistry in proto-planetary nebulae: detection of MgNC, NaCN, and AlF toward CRL 2688. *Astrophys. J.* **562**, 790–798 (2001).
19. Agúndez, M. et al. Molecular abundances in the inner layers of IRC 10216. *Astron. Astrophys.* **543**, A48 (2012).
20. Andreazza, C. M. & Almeida, A. A. D. The formation of AlF by radiative association. *Mon. Not. R. Astron. Soc.* **437**, 2932–2935 (2013).
21. Arnould, M., Goriely, S. & Jorissen, A. Non-explosive hydrogen and helium burnings: abundance predictions from the NACRE reaction rate compilation. *Astron. Astrophys.* **347**, 572–582 (1999).
22. Karakas, A. & Lattanzio, J. C. Stellar models and yields of asymptotic giant branch stars. *Publ. Astron. Soc. Aust.* **24**, 103–117 (2007).
23. Evans, A. et al. CK Vul: a smorgasbord of hydrocarbons rules out a 1670 nova (and much else besides). *Mon. Not. R. Astron. Soc.* **457**, 2871–2876 (2016).
24. Karakas, A. I. & Lugaro, M. Stellar yields from metal-rich asymptotic giant branch models. *Astrophys. J.* **825**, 26 (2016).
25. Politano, M., Sluys, M. V. D., Taam, R. E. & Willems, B. Population synthesis of common envelope mergers. I. Giant stars with stellar or substellar companions. *Astrophys. J.* **720**, 1752–1766 (2010).
26. Kochanek, C. S., Adams, S. M. & Belczynski, K. Stellar mergers are common. *Mon. Not. R. Astron. Soc.* **443**, 1319–1328 (2014).
27. Glassgold, A. E. ^{26}Al and circumstellar envelopes. *Astrophys. J.* **438**, L111–L114 (1995).
28. Indriolo, N. et al. Herschel survey of galactic OH^+, H_2O^+, and H_3O^+: probing the molecular hydrogen fraction and cosmic-ray ionization rate. *Astrophys. J.* **800**, 40 (2015).
29. Diehl, R. et al. Radioactive ^{26}Al from massive stars in the Galaxy. *Nature* **439**, 45–47 (2006).
30. Diehl, R. et al. INTEGRAL/SPI gamma-ray line spectroscopy. Preprint at https://arxiv.org/abs/1710.10139 (2017).
31. Hedderich, H. G. & Bernath, P. F. The infrared emission spectrum of gaseous AlF. *J. Mol. Spectrosc.* **153**, 73–80 (1992).
32. Hoeft, J., Lovas, F. & Tiemann, E. et al. Microwave absorption spectra of AlF, GaF, InF, and TlF. *Z. Naturforsch. A* **25**, 1029–1035 (2014).
33. Lide, D. R. High-temperature microwave spectroscopy. AlF and AlCl. *J. Chem. Phys.* **42**, 1013–1018 (1965).
34. Western, C. M. PGOPHER: a program for simulating rotational, vibrational and electronic spectra. *J. Quant. Spectrosc. Radiat. Transf.* **186**, 221–242 (2017).

35. Dunham, J. L. The energy levels of a rotating vibrator. *Phys. Rev.* **41**, 721–731 (1932).
36. Lutz, J. J. & Hutson, J. M. Deviations from Born–Oppenheimer mass scaling in spectroscopy and ultracold molecular physics. *J. Mol. Spectrosc.* **330**, 43–56 (2016).
37. McMullin, J. P., Waters, B., Schiebel, D., Young, W. & Golap, K. CASA architecture and applications. In *Astronomical Data Analysis Software and Systems XVI* (eds Shaw, R. A., Hill, F. & Bell, D. J.) 376 (Conference Series Volume 127, Astronomical Society of the Pacific, 2007).
38. Goodman, J. & Weare, J. Ensemble samplers with affine invariance. *Commun. Appl. Math. Comput. Sci.* **5**, 65–80 (2010).
39. Foreman-Mackey, D. et al. emcee: the MCMC hammer. *Publ. Astron. Soc. Pac* **125**, 306 (2013).
40. Goldsmith, P. F. & Langer, W. D. Population diagram analysis of molecular line emission. *Astrophys. J.* **517**, 209–225 (1999).
41. Gotoum, N., Hammami, K., Owono Owono, L. C. & Jaidane, N.-E. Collision induced rotational excitation of AlF ($X^1\Sigma^+$) by para-H_2 ($j=0$). *Astrophys. Space Sci.* **337**, 553–561 (2011).
42. Gotoum, N. et al. Rotational excitation of aluminium monofluoride (AlF) by He atom at low temperature. *Astrophys. Space Sci.* **332**, 209–217 (2010).
43. Lattanzio, J. C. The asymptotic giant branch evolution of 1.0–3.0 solar mass stars as a function of mass and composition. *Astrophys. J.* **311**, 708 (1986).
44. Karakas, A. I. Helium enrichment and carbon-star production in metal-rich populations. *Mon. Not. R. Astron. Soc.* **445**, 347–358 (2014).
45. Young, P. A. et al. Observational tests and predictive stellar evolution. *Astrophys. J.* **556**, 230 (2001).

Acknowledgements

We are grateful to the directors K. Schuster, P. Cox, S. Dougherty, T. van Zeeuw, R. Blundell and T. Beasley for granting us discretionary time at NOEMA, ALMA, APEX, SMA and JVLA. T.K. thanks L. Matrá for an introduction to Markov chain Monte Carlo methods. R.T. acknowledges support from grant 2017/27/B/ST9/01128, financed by the Polish National Science Centre. A.A.B. and T.F.G. acknowledge funding through the DFG priority programme 1573 (Physics of the Interstellar Medium) under grants GI 319/3-1 and GI 319/3-2, and the University of Kassel through P/1052 Programmlinie 'Zukunft'. K.T.W. acknowledges support from the International Max Planck Research School for Astronomy and Astrophysics at the Universities of Bonn and Cologne, and also from the Bonn–Cologne Graduate School of Physics and Astronomy. This study made use of APEX, which is a collaboration between the Max-Planck-Institut für Radioastronomie, European Southern Observatory and Onsala Space Observatory. Some of the APEX data were collected under the programmes 095.F-9543(A) and 296.D-5009(A). This paper makes use of the following ALMA data: ADS/JAO.ALMA#2015.A.00013.S and #2017.A.00030.S. ALMA is a partnership of ESO (representing its member states), NSF (USA) and NINS (Japan), together with NRC (Canada), NSC and ASIAA (Taiwan), and KASI (Republic of Korea), in cooperation with Chile. The Joint ALMA Observatory is operated by ESO, AUI/NRAO and NAOJ. The National Radio Astronomy Observatory is a facility of the National Science Foundation operated under cooperative agreement by Associated Universities. The IRAM 30 m observations were carried out under projects 183-14, 161-15 and D07-14, and those with NOEMA under W15BN, E15AE, S16AV and E16AC. IRAM is supported by INSU/CNRS (France), MPG (Germany) and IGN (Spain). The IRAM observations were supported by funding from the European Commission Seventh Framework Programme (FP/2007-2013) under grant agreement number 283393 (RadioNet3).

Author contributions

T.K. wrote the text and analysed the observations. A.A.B. and T.F.G. prepared the spectroscopic data. J.M.W. prepared, executed and calibrated the NOEMA observations. K.T.W. prepared and reduced the JVLA observations. T.K. prepared and reduced the ALMA and all single-dish observations. N.A.P. prepared and calibrated the SMA observations. R.T. and A.K. ran stellar-evolution models. All authors contributed to the interpretation of the data.

Competing interests

The authors declare no competing interests.

Additional information

Supplementary information is available for this paper at https://doi.org/10.1038/s41550-018-0541-x.

Reprints and permissions information is available at www.nature.com/reprints.

Correspondence and requests for materials should be addressed to T.K.

Publisher's note: Springer Nature remains neutral with regard to jurisdictional claims in published maps and institutional affiliations.